CEBAF Program Advisory Committee Six (PAC6) Proposal Cover Sheet

This proposal must be received by close of business on April 5, 1993 at:

CEBAF
User Liaison Office
12000 Jefferson Avenue
Newport News, VA 23606

Proposal Title

Extension of CEBAF E89-05
The Magnetic Form Factor of the Neutron
From the $d(\vec{e}, e'\vec{n})p$ Reaction

Contact Person

Name: R. Madey

Institution: Kent State University/Hampton University

Address: Physics Department

Address:

City, State ZIP/Country: Kent, Ohio 44242-0001 / Hampton, VA 23668

Phone: (216)-672-2596 / (804)-727-5277 **FAX:** (216)-672-2959 / (804)-727-5188

E-Mail → BITnet: **Internet:** IN%"MADEY@KSUVXA.KENT.EDU"
IN%"MADEY@CEBAF.GOV"

If this proposal is based on a previously submitted proposal or letter-of-intent, give the number, title and date:

CEBAF Use Only

Receipt Date: 4/5/93 Log Number Assigned: PR 93-039

By: gp

April 5, 1993

Extension of CEBAF E89-05

THE MAGNETIC FORM FACTOR OF THE NEUTRON FROM THE $d(\vec{e}, e'\vec{n})p$ REACTION

SCIENTIFIC PARTICIPANTS

Kent State Universtity

Kent, OH 44242

R. Madey (Spokesman)
B. Anderson
A. Baldwin
T. Eden
D. Keane
A. Lai
D. Manley
J. Watson
W. Zhang
Graduate Student(s)

CEBAF

Newport News, VA 23606

R. Carlini
D. Mack
J. Mitchell
P. Ulmer
R. Whitney
S. Wood
C. Yan

Hampton Universtity

Hampton, VA 23668

K. Baker
S. Beedoe
K. Beard
W. Buck
L. Tang
Graduate Student(s)

M.I.T.

Cambridge, MA 02139

W. Bertozzi
G. Dodson
M. Farkhondeh
W. Korsch
S. Kowalski
Graduate Student(s)

College of William and Mary
Williamsburg, VA 23185
M. Finn

Gettysburg College
Gettysburg, PA 17325
P. Pella

American University
Washington, DC 20016
B. Flanders

Duke University
Durham, NC 27707
C. Howell
W. Ternow
R. Walter
Graduate Student(s)

University of Virginia
Charlottesville, VA 22901
R. Lourie

I.U.C.F.
Bloomington, IN
J. Cameron

Old Dominion University
Norfolk, VA 23508
L. Weinstein

University of Maryland
College Park, MD 20742
C. Chang
J. Kelly
P. Markowitz

[This document was prepared by R. Madey, A. Lai, T. Eden, and W-M. Zhang of Kent State University.]

ABSTRACT

As an extension of CEBAF E89–05, we propose to determine the magnetic form factor G_M^n of the neutron in a model–insensitive way by scattering longitudinally–polarized electrons from deuterium quasielastically and measuring the transverse polarization component $P_{S'}$ of the recoil neutron in coincidence with the scattered electron, and by making another measurement of the scaled cross section I_o $[= (1+\tau)\sigma(\theta_e)/\sigma_{Mott}(\theta_e)]$ for elastic scattering of unpolarized electrons from unpolarized neutrons. In the proposal for CEBAF E89–05, we described in detail the measurement of the neutron polarization component $P_{S'}$ [or the polarization–transfer coefficient $D_{LS'}(= P_{S'}/P_L)$] from the $d(\vec{e},e'\vec{n})p$ reaction, which will determine the ratio ($g \equiv G_E^n/G_M^n$) of the neutron electric form factor G_E^n to G_M^n at five values of the four–momentum transfer–squared, [viz., $Q^2 = 0.30$, 0.50, 1.0, 1.5, and 2.0 (GeV/c)^2]. By restricting the horizontal angular acceptance of the electron spectrometer, we can determine G_M^n with a relative statistical uncertainty that is given essentially by one half of the relative uncertainty in I_o. In addition to obtaining independent and model–insensitive values of G_M^n, agreement with expected G_M^n values provides an internal consistency check on our extracted values of G_E^n. Also, we can preserve the model insensitivity of our G_E^n measurements by using our own model-insensitive values of G_M^n to obtain G_E^n.

Current values of G_M^n have been extracted from the cross sections of quasielastic or elastic electron–deuteron scattering experiments, which are sensitive to the deuteron wavefunction, final-state interactions (FSI), meson-exchange currents (MEC), and a parameterization for G_E^n. In the proposed Q^2 region in comparison with lower Q^2, the relative contribution to the cross section depends more sensitively on the assumed value of G_E^n as shown in Table IV; in the dipole parameterization of G_E^n, for example, the relative contribution of G_E^n can be a significant fraction of that associated with G_M^n. The experiment proposed here will provide *model–insensitive* results with statistical uncertainties that are comparable to (or smaller than) those of the best measurements performed thus far.

TABLE OF CONTENTS

LIST OF TABLES

LIST OF FIGURES

CEBAF E89-05 EXTENSION

The Magnetic Form Factor of the Neutron from the $d(\vec{e}, e'\vec{n})p$ Reaction

1. Scientific Background and Motivation

The electric form factor G_E^n of the neutron is a fundamental quantity needed for the understanding of both nucleon and nuclear structure. Because extracting G_E^n from the polarization–transfer reaction $d(\vec{e}, e'\vec{n})p$ is model insensitive,[1–4] we desire to take the advantage of this model insensitivity to measure the magnetic form factor of the neutron G_M^n via polarization–transfer on deuterium. Because G_E^n is directly proportional to G_M^n, a model–insensitive measurement of G_M^n can only sustain the complete model insensitivity of G_E^n.

We propose to measure G_M^n at the same five Q^2 values as those proposed for measuring G_E^n in CEBAF E89–05 [*viz.*, Q^2 = 0.30, 0.50, 1.0, 1.5, and 2.0 $(\mathrm{GeV}/c)^2$]. We will show in this proposal that we can extract G_M^n in a model–insensitive way from the polarization–transfer coefficient $D_{LS'}$ (which we are measuring to extract G_E^n) and the scaled cross section I_o. By restricting the horizontal angular acceptance of the electron spectrometer in a separate measurement of I_o, we will show also that we can determine G_M^n with a relative uncertainty that is given essentially by one–half of the relative uncertainty in the neutron detection efficiency. By extracting G_M^n from $D_{LS'}$ (and I_o) and obtaining the expected value of G_M^n, we provide an internal consistency check on our value of G_E^n, which is extracted from the same $D_{LS'}$. This internal consistency check adds confidence to the G_E^n results from our polarization–transfer measurements in CEBAF E89-05.

Our goals of performing this experiment are three fold: *One,* we want to provide an internal consistency check on our extracted values of G_E^n; *two,* we want to map out G_M^n in a model–independent fashion at the corresponding Q^2–points that are part of our G_E^n proposal; and *three,* we want to preserve the model–insensitivity of our G_E^n measurements by using our own model–independent values of G_M^n to compute G_E^n.

The published data that currently make up the world's data set for G_M^n are tabulated in Appendix A. Current values of G_M^n have been extracted from quasielastic and elastic e–d scattering.[5–14] For $Q^2 < 1.0$ (GeV/c)^2, the measurements on G_M^n with the smallest (statistical only) uncertainties were performed by Esaulov *et al.*[6] (1987), resulting in relative uncertainties in G_M^n from $\sim$ 3% to $\sim$ 5%. For Q^2 between 1.0 and 2.0 (GeV/c)^2, Lung *et al.*[5] (1993) measured G_M^n at $Q^2 = 1.75$ (GeV/c)^2 with a relative uncertainty 5.1%. Earlier measurements by Bartel *et al.*[7] had relative statistical uncertainties $\Delta G_M^n/G_M^n$ = 8.0, 5.5, and 5.2% for $Q^2 = 0.565$, 1.0, and 1.53 (GeV/c)^2, respectively; and Hanson *et al.*[8] (1973) had $\Delta G_M^n/G_M^n$ = 4.4 and 7.2% for $Q^2 = 1.17$ and 1.755 (GeV/c)^2, respectively. Other measurements at Q^2 between 1.0 and 2.0 (GeV/c)^2 have larger uncertainties. *These analyses*, as described below, *suffer from systematic uncertainties from deuteron structure that are not understood completely.* Model–independent measurements of G_M^n do not exist for any Q^2.

Four techniques have been used to extract G_M^n from quasielastic e–d scattering:

1. Inclusive quasielastic e–d scattering: Subtract the proton contribution from the measured $d(e,e')np$ cross section and perform a separation of the longitudinal and transverse pieces of the remaining cross section to obtain the magnetic contribution.

2. Measurement of the exclusive $d(e,e'n)p$ cross section.

3. Quasi–coincidence experiments involving the reaction $d(e,e'p^\star)n$, where $p^\star$ means that the proton is not detected. Here one avoids the detection of the neutron by detecting the absence of a recoil proton in the direction of $\vec{q}$. Exclusion of the $d(e,e'p)$ reaction implies that the observed reaction is $d(e,e'n)p$.

4. Extraction of G_M^n from the ratio of the $d(e,e'n)p$ and $d(e,e'p)n$ cross section.

For inclusive quasielastic e–d scattering, uncertainties originate from the subtraction of the dominant $p(e,e')$ contribution from the $d(e,e')np$ cross section.

A longitudinal/transverse Rosenbluth separation of the remaining cross section is performed to extract G_M^n. In obtaining the remaining cross section from the residual (after subtraction) angular distribution, theoretical uncertainties can stem also from the integration of the remaining inclusive cross section over the entire quasielastic peak. The fraction of strength that can be neglected (from the wings in the quasielastic peak) depends on the deuteron wave function, meson–exchange currents (MEC), and final–state interactions (FSI). Recently, Lung *et al.*[5] reported an insensitivity of G_M^n to deuteron wave functions in their analysis; however, they did not examine effects from FSI and MEC. Another study by Esaulov *et al.*,[6] shows that *the value of the extracted G_M^n and its uncertainty depend on the amount of D–state strength that appears in the deuteron wave function.* Shown in Table I for $Q^2 = 0.482$ and 0.832 $(\mathrm{GeV}/c)^2$ are values of G_M^n extracted from three deuteron wavefunctions with different D–state probabilities P_D: Reid[15] ($P_D = 6.47\%$), Paris[16] ($P_D = 5.77\%$), and the Buck and Gross[17] deuteron wavefunction ($P_D = 4.74\%$).

Table I. Values of G_M^n/μ_n Procured from Different Deuteron Wave Functions

Q^2 $(\mathrm{GeV}/c)^2$	Reid Potential ($P_D = 6.47\%$)	Paris Potential ($P_D = 5.77\%$)	Buck–Gross DWF ($P_D = 4.74\%$)
0.482	0.649	0.638	0.607
0.832	0.232	0.229	0.220

Note that these values for G_M^n impose the dipole parameterization for $G_E^n (\equiv -\tau G_M^n)$.

Exclusive $d(e, e'n)p$ cross sections have been measured to an accuracy of about 5–6% for low Q^2 ($Q^2 < 0.30$ $(\mathrm{GeV}/c)^2$)[18] and to about 10%[19] for large Q^2. At low Q^2, this technique is valid because the relative contribution to the cross section associated with G_E^n is small. For higher Q^2, this technique is more sensitive to the parameterization of G_E^n; for example, for the dipole parameterization of G_E^n, the

contribution to the cross section increases with increasing Q^2. The experiments need to know the neutron detection efficiency. Extracting G_M^n by this technique demands an investigation of the response of G_M^n with respect to different N–N potentials for a particular parameterization of G_E^n.

The third method requires an excellent understanding of the reaction mechanism to be able to deal with all processes that can lead to an absence of a proton in the direction of $\vec{q}$.[8] Again, MEC and FSI effects needs to be understood well in order to use the full quasielastic peak. Restricting the analysis to the top of the quasielastic peak induces sensitivity with respect to the deuteron wave function. In general, extracting a small contribution from $d(e,e'n)p$ from two large processes [*viz.*, $d(e,e'p)$ and $d(e,e'p^*)$] can lead to large systematic uncertainties.

At the quasielastic peak, the ratio method has been employed in the past[7,11] with resulting uncertainties at about the 10% level. Briefly, at the quasielastic peak, this ratio *should* be equal to the ratio of the free electron–neutron to electron–proton cross sections:

$$R \approx \frac{(G_M^n)^2 \left[\frac{\left(G_E^n/G_M^n\right)^2 + \tau}{1+\tau} + 2\tau \tan^2(\theta_e/2) \right]}{(G_M^p)^2 \left[\frac{\left(G_E^p/G_M^p\right)^2 + \tau}{1+\tau} + 2\tau \tan^2(\theta_e/2) \right]} \quad . \tag{1}$$

Here the neutron cross sections were deduced from R by making use of the more accurately determined proton form factors. It was believed that taking into account nuclear effects related to the structure of the deuteron (*viz.*, deuteron wave functions, MEC, and FSI) does not present fundamental difficulties; however, as pointed out by Esaulov *et al.*,[6] *theoretical and experimental studies of recent years have shown that the deuteron is not as simple a system as previously thought.* By including the large quasifree scattering contribution from the proton, additional uncertainties involving cancellations of nuclear effects between both cross sections in the ratio R is not very clear. In order to suppress theoretical uncertainties as far as possible, it is necessary to restrict the analysis to the top of the quasielastic peak.

Here supposedly, MEC effects are small, but FSI interactions need to be calculated accurately for both cross sections; in addition, an uncertainty with respect to the parameterization of G_E^n can induce systematic error in extracting G_M^n. The ratio technique for measuring G_M^n has been used in experiments (with results not yet reported) at NIKHEF and BONN and in a planned experiment at Mainz.

To extract G_M^n in these experiments, it is necessary to choose a particular deuteron wave function and a parameterization for G_E^n. In the region of four-momentum transfer-squared Q^2 that we plan to perform our measurements, the choice of parameterization for G_E^n affects the extracted value of G_M^n. In Fig. 1, we show published results of G_M^n measurements in the Q^2 region up to 2.0 $(\mathrm{GeV/c})^2$. One of our ultimate goals, as proposed for CEBAF E89-05, is to measure G_E^n in a model-insensitive way. Because G_E^n is directly propotional to G_M^n, the value of G_E^n will be affected also by the existing *model-dependent* values of G_M^n. By extracting G_M^n from polarization-transfer on deuterium, we show in this proposal that G_M^n will be free of such systematic influences; and consequently, the model independence of G_E^n is preserved.

Because each of the above four techniques requires knowledge about deuteron structure, the results suffer from systematic uncertainties that can't be avoided; for this reason, a measurement of G_M^n by a model-insensitive polarization-transfer technique is attractive. By obtaining G_M^n from the polarization-transfer coefficient $D_{LS'}$, the dependence on the deuteron structure is dynamically small and well understood; the effects of MEC, FSI, and isobar configurations (IC) on $D_{LS'}$ are negligible for quasifree kinematics. We are able to design the experiment so that the relative uncertainty in the neutron detection efficiency enters into ΔG_M^n as one half of its true value. Thus, obtaining G_M^n by polarization-transfer on deuterium will reduce the systematic uncertainties that plague previous experiments.

2. Measurement of G_M^n (and G_E^n) with a Neutron Polarimeter

2.1 Introduction

Electron scattering is an effective means to probe the substructure of nucleons and nuclei. For an unpolarized electron scattered from an unpolarized neutron, the cross section can be written

$$\sigma(\theta_e) \equiv \frac{d\sigma}{d\Omega_e} = \frac{\sigma_{Mott}}{1+\tau}\ \left[(G_E^n)^2 + B(\theta_e)(G_M^n)^2\right]\ . \tag{2}$$

Here the Mott cross section is given by

$$\sigma_{Mott}(\theta_e) = \left(\frac{\alpha^2}{Q^2}\right)\left(\frac{E'}{E}\right)^2\ \cot^2\left(\frac{\theta_e}{2}\right) \tag{3}$$

with

$$Q^2 = 4EE'\sin^2\left(\frac{\theta_e}{2}\right) \tag{4}$$

and

$$\frac{E'}{E} = \frac{1}{1+2(E/M)\sin^2(\theta_e/2)}. \tag{5}$$

The kinematic function $B(\theta_e)$ is given by

$$B(\theta_e) = \tau + \frac{1}{2}A^2(\theta_e) \qquad (\tau = \frac{Q^2}{4M^2}) \tag{6}$$

with

$$A(\theta_e) \equiv 2\sqrt{\tau(1+\tau)}\tan(\frac{\theta_e}{2})\,. \tag{7}$$

Now, we define a *scaled cross section* I_o:

$$I_o \equiv \frac{\sigma(\theta_e)}{\sigma_{Mott}(\theta_e)}(1+\tau) = (G_E^n)^2 + B(\theta_e)\,(G_M^n)^2\,, \tag{8}$$

such that

$$\sigma(\theta_e) \equiv \frac{d\sigma}{d\Omega_e} = \frac{\sigma_{Mott}}{1+\tau}\,I_o\,. \tag{9}$$

In Fig. 2 for $Q^2 = 1.0$ (GeV/c)^2, we plot the cross section $d\sigma/d\Omega_e$ and the scaled cross section I_o as a function of electron scattering angle θ_e for the Galster param-

eterization of G_E^n [$g \equiv G_E^n/G_M^n = -\tau/(1+5.6\tau)$], the dipole parameterization of G_E^n [$g = -\tau$], and $g = 0$. Equation (9) indicates that a measurement of the cross section $d\sigma/d\Omega_e$ will enable us to extract the scaled cross section I_o, which in turn provides useful information about the form factors G_E^n and G_M^n. Although a measurement of I_o alone is not sufficient for the extraction of either G_E^n or G_M^n, it was suggested by Arnold, Carlson, and Gross[20] (1981) that the ratio $G_E^n/G_M^n \equiv g$ can be determined by measuring the transverse polarization $P_{S'}$ of the recoil neutron after quasielastic scattering of a longitudinally–polarized electron from an unpolarized neutron. In the poposal for CEBAF E89–05, we described in detail how we can determine the ratio $g \equiv G_E^n/G_M^n$ by measuring $P_{S'}$ or the polarization–transfer coefficient $D_{LS'} \equiv P_{S'}/P_L$. We obtained the result that

$$g \equiv \frac{G_E^n}{G_M^n} = \frac{(A^2 - 4BD_{LS'}^2)^{1/2} - A}{2D_{LS'}}, \tag{10}$$

Now if we measure I_o also, we will have enough information to extract G_M^n as well as G_E^n, as we will show in the next section. We will show also that the measurement can be designed so that the relative statistical uncertainty $\Delta G_M^n/G_M^n$ is given to a good approximation by one-half of the relative statistical uncertainty in the scaled cross section; that is

$$\frac{\Delta G_M^n}{G_M^n} \simeq \frac{1}{2}\frac{\Delta I_o}{I_o}. \tag{11}$$

2.2 Neutron Form Factors and Their Uncertainties

From Eq. (8), we have

$$(G_M^n)^2 = \frac{I_o}{B+g^2} = I_o \frac{2D_{LS'}^2}{A(A - \sqrt{A^2 - 4BD_{LS'}^2})}, \tag{12}$$

and

$$(G_E^n)^2 = g^2\,(G_M^n)^2 = I_o \frac{A - \sqrt{A^2 - 4BD_{LS'}^2}}{2A}. \tag{13}$$

Now, we can rewrite Eqs. (12) and (13):

$$(G_X^n)^2 \equiv I_\circ f_X^n \qquad (X = E, M) \tag{14}$$

with

$$X = E: \qquad f_E^n = \frac{A - \sqrt{A^2 - 4BD_{LS'}^2}}{2A} \tag{15}$$

$$X = M: \qquad f_M^n = \frac{2D_{LS'}^2}{A(A - \sqrt{A^2 - 4BD_{LS'}^2})}. \tag{16}$$

The uncertainties for the form factors can be written as:

$$\frac{\Delta G_X^n}{G_X^n} = \frac{\Delta (G_X^n)^2}{2(G_X^n)^2} = \left[\left(\frac{\Delta f_X^n}{2f_X^n}\right)^2 + \left(\frac{\Delta I_\circ}{2I_\circ}\right)^2\right]^{1/2} \qquad (X = E, M), \tag{17}$$

where

$$\left(\frac{\Delta f_X^n}{f_X^n}\right)^2 = \left(\frac{D_{LS'}\partial \ln f_X^n}{\partial D_{LS'}}\right)^2 \left(\frac{\Delta D_{LS'}}{D_{LS'}}\right)^2 + \left(\frac{A\partial \ln f_X^n}{\partial A}\frac{d\ln A}{d\theta_e} + \frac{B\partial \ln f_X^n}{\partial B}\frac{d\ln B}{d\theta_e}\right)^2 (\Delta\theta_e)^2. \tag{18}$$

All the partial derivatives in this equation can be expressed in terms of the function f_1 ($\equiv A/\sqrt{A^2 - 4D_{LS'}^2 B}$), which was defined in the proposal for CEBAF E89–05, because of the following indentities:

$$\frac{D_{LS'}\partial \ln(A - \sqrt{A^2 - 4BD^2})}{\partial D_{LS'}} = f_1 + 1, \tag{19}$$

$$\frac{A\partial \ln(A - \sqrt{A^2 - 4BD_{LS'}^2})}{\partial A} = -f_1, \tag{20}$$

$$\frac{B\partial \ln(A - \sqrt{A^2 - 4BD_{LS'}^2})}{\partial B} = \frac{1}{2}(f_1 + 1). \tag{21}$$

These expressions lead to

$$\frac{D_{LS'}\,\partial \ln f_E^n}{\partial D_{LS'}} = (f_1+1), \quad \frac{A\,\partial \ln f_E^n}{\partial A} = -(f_1+1), \quad \frac{B\,\partial \ln f_E^n}{\partial B} = \frac{1}{2}(f_1+1); \quad (22)$$

$$\frac{D_{LS'}\,\partial \ln f_M^n}{\partial D_{LS'}} = -(f_1-1), \quad \frac{A\,\partial \ln f_M^n}{\partial A} = (f_1-1), \quad \frac{B\,\partial \ln f_M^n}{\partial B} = -\frac{1}{2}(f_1+1). \quad (23)$$

Now, with the definition

$$x_\pm \equiv \frac{f_1 \pm 1}{2}, \quad (24)$$

we can express the relative statistical uncertainties in the form factors in terms of the following psuedo-symmetric formulas:

$$\frac{\Delta G_E^n}{G_E^n} = \left[x_+^2 \left(\frac{\Delta D_{LS'}}{D_{LS'}}\right)^2 + \left(x_+ \frac{d\ln A}{d\theta_e} - x_+ \frac{d\ln B}{2d\theta_e}\right)^2 (\Delta\theta_e)^2 + \left(\frac{\Delta I_o}{2I_o}\right)^2 \right]^{\frac{1}{2}}, \quad (25)$$

$$\frac{\Delta G_M^n}{G_M^n} = \left[x_-^2 \left(\frac{\Delta D_{LS'}}{D_{LS'}}\right)^2 + \left(x_- \frac{d\ln A}{d\theta_e} - x_+ \frac{d\ln B}{2d\theta_e}\right)^2 (\Delta\theta_e)^2 + \left(\frac{\Delta I_o}{2I_o}\right)^2 \right]^{\frac{1}{2}}. \quad (26)$$

The expressions for the complete derivatives $d\ln A/d\theta_e$ and $d\ln B/d\theta_e$ are given in Eqs. (18) and (19) respectively in the proposal for CEBAF E89–05.

In summary, by measuring the polarization–transfer coefficient $D_{LS'}$ with a relative uncertainty $\Delta D_{LS'}/D_{LS'}$ and the scaled cross section I_o with a relative uncertainty $\Delta I_o/I_o$, we can extract G_E^n and G_M^n from Eqs. (12) and (13) with their relative statistical uncertainties calculated by Eqs. (25) and (26).

Several points should be made about the uncertainty calculations.

• 1. Apparently, the uncertainty $\Delta G_E^n/G_E^n$ calculated by Eq. (25) will not be the same as that calculated in the proposal for CEBAF E89–05 [from Eq. (74) together with Eqs. (24), (25), (26), and (27) in that proposal]. In that proposal,

we assumed a relative uncertainty on G_M^n of 2.5%. In this proposal extension, we assume three different values of $\Delta I_o/I_o$, *i.e.*, $\Delta I_o/I_o = 0.10$, 0.075, and 0.050 to make comparisons between the two different calculations of $\Delta G_E^n/G_E^n$. It is found that both methods give similar numerical results. We list these results In Table II for $Q^2 = 1.0$ (GeV/c)^2.

Table II. Comparison of Uncertainties in G_E^n for $Q^2 = 1.0$ (GeV/c)^2

	$\Delta G_E/G_E$ (%)			
$\Delta I_o/I_o$	Galster		Dipole	
0.10	16.8*	18.1†	13.2*	14.3†
0.075	16.8*	17.8†	13.2*	13.9†
0.050	16.8*	17.6†	13.2*	13.7†

* Calculated from Eq. (74) in the proposal for CEBAF E89–05 with an assumed $\Delta G_M^n/G_M^n = 0.025$.

† Calculated from Eq. (25) in this proposal.

Results for other proposed Q^2 points have the same conclusion. This conclusion indicates that we can calculate the uncertainties for G_E^n by either method depending on the actual design for the experiment. It should be noted that the variation of $\Delta I_o/I_o$ between 0.05 and 0.10 (a practically achievable region) does not affect the value of $\Delta G_E^n/G_E^n$ significantly because the dominating contribution to $\Delta G_E^n/G_E^n$ for this range of values for $\Delta I_o/I_o$ comes from the term $x_+^2(\Delta D_{LS'}/D_{S'})^2$, which will not be the case for the uncertainty $\Delta G_M^n/G_M^n$ as discussed below.

• 2. In Fig. 3 for $Q^2 = 1.0$ (GeV/c)^2, we plot the contributions to the squared uncertainty $(\Delta G_M^n/G_M^n)^2$ for both the dipole and the Galster parameterizations of G_E^n, where the kinematic conditions and acceptances are those given in the proposal for CEBAF E89–05. It shows clearly that the major contributions to

the overall uncertainty in G_M^n are those associated with $\Delta\theta_e$ ($= \pm$ 3.40° in this plot) and $\Delta I_o/I_o$ ($= \pm$ 0.10 in this plot), while the contribution from the term $x_-^2(\Delta D_{LS'}/D_{LS'})^2$ is very small. The same conclusion also holds for other proposed Q^2 points. This result can be understood by noticing that the function $x_- = (f_1-1)/2$ in front of $\Delta D_{LS'}/D_{LS'}$ in Eq. (25) is small because f_1 has values of order unity in our kinematic region. [Note that $x_+ = (f_1+1)/2$ (instead of x_-) is in front of $\Delta D_{LS'}/D_{LS'}$ in Eq. (25) for the uncertainty in G_E^n, which makes the term $x_+^2(\Delta D_{LS'}/D_{LS'})^2$ the domimating contribution to the uncertainty in G_E^n]. The fact that the major contributions to the uncertainty in G_M^n are from $\Delta I_o/I_o$ and the term associated with $\Delta\theta_e$ indicates that further improvement in terms of reducing the uncertainties can be made by reducing $\Delta\theta_e$ or $\Delta I_o/I_o$. Later in this proposal extension, we will show that the uncertainty $\Delta I_o/I_o$ can depend significantly on the electron angular acceptance $\Delta\theta_e$; therefore, by reducing $\Delta\theta_e$, we will reduce both uncertainties from the direct $\Delta\theta_e$ term and the $\Delta I_o/I_o$ term. To measure the scaled double–coincidence cross section I_o, we plan to insert a collimator into the high–momentum spectrometer (HMS) to reduce the electron angular acceptance. In Table III, we give the uncertainties in G_M^n (with $\Delta\theta_e = \pm 3.40°$ before inserting the collimator) for the five proposed Q^2 points assuming three different values of $\Delta I_o/I_o$; in calculating these uncertainties, the same relative uncertainties on $D_{LS'}$ and angular acceptances are used as those in the proposal for CEBAF E89–05.

It should be emphasized again that the projected uncertainties in Table III are associated with an electron angular acceptance of $\Delta\theta_e = \pm$ 3.40° which was chosen to optimize the data taking process in the triple–coincidence mode for the G_E^n measurement. This $\Delta\theta_e$ can be reduced further for the data in double coincidence mode (for the measurement of the scaled cross section I_o).

Table III. Projected Uncertainties on G_M^n with $\Delta\theta_e = \pm\ 3.40°$

			$\Delta G_M^n/G_M^n$ (%)						
Q^2	θ	E	$\frac{\Delta I_o}{I_o}$:	0.10		0.075		0.050	
$(\mathrm{GeV/c})^2$	(deg)	(GeV)		G*	D*	G*	D*	G*	D*
2.0	46.6	2.4		7.8	7.6	7.1	6.8	6.5	6.2
1.5	65.5	1.6		6.9	6.7	6.1	5.9	5.4	5.2
1.0	45.0	1.6		7.9	7.1	7.2	6.3	6.7	5.7
0.5	65.5	0.8		7.1	7.0	6.3	6.1	5.6	5.4
0.3	45.0	0.8		8.4	8.2	7.7	7.5	7.2	7.0

* G: for G_E^n in Galster parameterization D: for G_E^n in Dipole parameterization.

• 3. The disadvantage of this technique is that it requires a determination of the neutron detection efficiency to extract the relative uncertainty $\Delta I_o/I_o$; however, it is not a unique problem associated with this technique.

• 4. It should be pointed out that the most obvious advantage of the technique suggested here is that it provides a measurement of G_M^n that is model insensitive. In our previous (Bates E85–05 extension) experiment, we used a different technique to obtain the value of G_M^n for $Q^2 \leq 0.25$ $(\mathrm{GeV}/c)^2$; that is, we measured the $d(e,e'n)p$ coincidence cross section and extracted G_M^n by preassuming a G_E^n value such as that given by the Galster parameterization. This technique is valid for low Q^2 values because the relative contribution to the cross section associated with G_E^n is only $\sim 3\%$ of that associated with G_M^n for $Q^2 \lesssim 0.25$ $(\mathrm{GeV}/c)^2$, with the result that the assumed value of G_E^n introduces only small a uncertainty in G_M^n; however, this technique may no longer be reliable for higher Q^2 because the relative contribution to the value of the cross section associated with G_E^n is large. In Table IV we show the relative contribution of various G_E^n parameterizations to the cross section for the five Q^2 points in CEBAF proposal E89–05.

Table IV. Contribution of G_E^n to the Cross Section

Q^2 (GeV/c)^2	θ_e (deg)	$B(\theta_e)$	$\frac{I_o}{B(G_M^n)^2}$; $(g = -\tau)$ Dipole	$\frac{I_o}{B(G_M^n)^2}$; $[g = -\tau(1+5.6\tau)^{-1}]$ Galster
0.30	45.1	0.1167	6.2%	2.8%
0.50	65.7	0.2764	7.3%	2.3%
1.00	45.0	0.4079	19.7%	2.9%
1.50	65.6	0.9256	19.5%	1.7%
2.00	46.6	0.8955	35.8%	2.1%

For the point at $Q^2 = 1.0$ (GeV/c)^2 with the dipole parameterization of G_E^n, the relative contribution to the cross section associated with G_E^n would be $\sim$ 20% of that associated with G_M^n for a relatively large scattering angle ($\theta_e = 45°$) proposed for the G_E^n experiment, while the same relative contribution from G_E^n is only about $\sim$ 3% of that with the Galster parameterization; in other words, at higher Q^2 values the relative contribution from G_E^n to the cross section has a larger sensitivity to the model assumed for G_E^n. To extract G_M^n from the measured cross section by preassuming a value for G_E^n will introduce larger uncertainties at the higher Q^2 values than at the lower Q^2 values. With the technique suggested here, we do not need to assume a value for G_E^n to extract G_M^n. The polarization-transfer measurement of $D_{LS'}$ is model-insensitive (as pointed out in the proposal for CEBAF E89–05), and the value of I_o is obtained from a measurement.

3. Experimental Arrangement

In the proposal for CEBAF E89–05 Section 3, we presented a detailed description of the neutron polarimeter and its steel collimator and shielding enclosure.

We plan to measure I_o in two ways:

The first way is to measure I_o *simultaneously* with the measurement of $P_{S'}$. This method does not require additional data acquisition time because we add an-

other neutron detector ahead of the analyzing detectors of the neutron polarimeter. We measure I_o from the double-coincidence events of neutrons in this detector with electrons in the high-momentum spectrometer (HMS). We design this I_o neutron detector so that the double-coincidence rate will be comparable with the triple-coincidence rate for the measurement of the polarization-transfer coefficient. We plan to limit the horizontal angular acceptance $\Delta\theta_n$ of this additional neutron detector to be about one fourth of that of the original neutron polarimeter employed for the $P_{S'}$ measurement. Although it may not result in an uncertainty in G_M^n as small as desired, it does not require additional data acquisition time. This method will serve as a pre–check of the second method, which will lead to a more precise measurement of G_M^n.

The second way is to measure I_o separately. The advantage of a separate measurement is that we can further collimate the HMS to reduce the electron angular acceptance to achieve the desired uncertainties in G_M^n. In the next section, we discuss the experimental design and estimate the uncertainties achievable with praticable data acquisition times. Obviously, this separate measurement requires some additional beam time. Because this measurement requires only double coincidence events, we can obtain the number of events required for a small relative uncertainty even with the smaller angular acceptances.

4. Design of the Experiment

In the proposal for CEBAF E89–05, we presented a detailed description of the measurement of $P_{S'}$. In this section, we will concentrate on the issues related to the measurement of the scaled cross section I_o, as discussed in the second technique above.

4.1 Data Acquisition in Triple– and Double–Coincidence Modes

We plan to take data for the triple- and the double-coincidence events. The triple–coincidence data will be used to extract the transverse polarization $P_{S'}$ (or the polarization transfer coefficient $D_{LS'}$), and the double–coincidence data will be

used to compute the scaled cross section I_o. Also, a polarized electron beam will be used for taking the triple–coincidence data to measure $P_{S'}$, and an unpolarized electron beam for the double–coincidence data to measure I_o. For the triples–mode, we will keep the angular acceptances as designed in the proposal for CEBAF E89–05, *i.e.*, $\Delta\theta_e = \pm\ 3.40°$, and $\Delta\theta_n = \pm\ 3.00°$. For the doubles–mode, we plan to decrease the angular acceptances by a factor of four for the first method, and to collimate the HMS such that the angular acceptance $\Delta\theta_e$ is on the order of $\pm\ 0.3°$ for the second method.

4.2 The Scaled Singly – Differential Cross Section and Its Uncertainty

Although a single-arm cross section $d\sigma/d\Omega_e$ is required to extract the scaled cross section I_o, it should be noted that the number of electrons needed to compute the single arm cross section from the reaction $d(e,e'n)p$ still have to be counted in coincidence with neutrons because otherwise the electrons may be associated with protons from the reaction $d(e,e'p)n$. This fact requires that we must obtain the singly–differential cross section $d\sigma/d\Omega_e$ associated with the reaction $d(e,e'n)p$ from the measured number of electrons, N_e, that are detected in the HMS in coincidence with a neutron in one or more of the analyzing detectors of the neutron polarimeter. The true number of neutrons N_n (or *yield* $\equiv Y$) is given by

$$N_n \equiv Y = \frac{N_{double}}{\epsilon_n\ \epsilon_{rc}}\ , \tag{27}$$

where N_{double} is the number of neutrons actually detected in coincidence with an electron, ϵ_n is the neutron detection efficiency, and ϵ_{rc} is the radiative correction factor with a value less than unity. The true number of electrons in the electron arm, N_e, must be equal to the true number of neutrons in the neutron arm because of the requirement stated in above:

$$N_e = N_n = \frac{N_{double}}{\epsilon_n\ \epsilon_{rc}}\ . \tag{28}$$

Then, the measured singly-differential cross section is simply

$$\frac{d\sigma}{d\Omega_e} = \left(\frac{N_e}{L_{int.}}\right)\left(\frac{1}{\Delta\Omega_e}\right) = \left(\frac{N_{double}}{\epsilon_n\ \epsilon_{rc}}\right)\left(\frac{1}{L_{int.}}\right)\left(\frac{1}{\Delta\Omega_e}\right). \tag{29}$$

Here the integrated luminosity $L_{int.}$ is given by

$$L_{int.} = \left(\frac{Q}{e}\right)\left(\frac{t\,N_A}{A}\right), \tag{30}$$

where $Q = \int_0^T I\,dt$ is the total charge collected in the incident beam during the data aquisition period T, e is the electron charge, t is the target thickness, A is the atomic number of the target (= 2.01 for deuteron), and N_A is Avogadro's number. In fact, Eq. (29) can also be obtained from

$$\frac{d\sigma}{d\Omega_e} = \int \frac{d^3\sigma}{d\Omega_e d\Omega_n dp_e} d\Omega_n dp_e = \langle\sigma_3\rangle\,\Delta\Omega_n\Delta p_e \tag{31}$$

with

$$\langle\sigma_3\rangle = \left(\frac{N_{double}}{\epsilon_n\,\epsilon_{rc}}\right)\left(\frac{1}{L_{int.}}\right)\left(\frac{1}{\Delta\Omega_e\Delta\Omega_n\Delta p_e}\right). \tag{32}$$

Now, the measured scaled cross section I_o is

$$I_o \equiv \left(\frac{d\sigma}{d\Omega_e}\right)\left(\frac{1+\tau}{\sigma_{Mott}}\right) = \left(\frac{N_{double}}{\epsilon_n\,\epsilon_{rc}}\right)\left(\frac{1}{L_{int.}}\right)\left(\frac{1}{\Delta\Omega_e}\right)\left(\frac{1+\tau}{\sigma_{Mott}}\right). \tag{33}$$

The right hand member in this equation follows from Eq. (29).

Now, we want to estimate the uncertainty on I_o. Because the integrated luminosity $L_{int.}$ can be measured with precision, and because σ_{Mott} is the only θ_e-dependent quantity in Eq. (33), this scaled cross section can be conveniently written in the following simplified form:

$$I_o = \lambda f(\theta_e)\left(\frac{N_{double}}{\epsilon_n}\right), \tag{34}$$

where $\lambda = 4E^2/(M^2\alpha^2\epsilon_{rc}\,L_{int.}\,\Delta\Omega_e)$ is a constant for known electron beam energy E, radiative correction factor ϵ_{rc}, integrated luminosity $L_{int.}$, and solid-angle

acceptance $\Delta\Omega_e$. The function $f(\theta_e)$ is given by

$$f(\theta_e) = \left[M^2 + (M+E)^2 \tan^2(\theta_e/2)\right] \sin^4(\theta_e/2). \tag{35}$$

The relative uncertainty in I_o is

$$\frac{\Delta I_o}{I_o} = \left[\left(\frac{\Delta N_{double}}{N_{double}}\right)^2 + \left(\frac{\Delta\epsilon_n}{\epsilon_n}\right)^2 + h^2(\theta_e)(\Delta\theta_e)^2\right]^{1/2} \tag{36}$$

with

$$h(\theta_e) \equiv \frac{\partial f}{f\partial\theta_e} = 2\cot\frac{\theta_e}{2} + \frac{(M+E)^2\sin(\theta_e)}{\cos^3(\theta_e/2)[M^2 + (M+E)^2\tan^2(\theta_e/2)]} \tag{37}$$

In Eq. (36), the term $(\Delta N_{double}/N_{double})^2$ is determined by statistics, which can be as small as desired in principle; the term $[h(\theta_e)\Delta\theta_e]^2$ can be reduced by reducing $\Delta\theta_e$; the term $(\Delta\epsilon_n/\epsilon_n)^2$ can be either measured or calculated. Considering that the calculation or determination of the neutron detection efficiency may involve an uncertainty as high as 10%, we want to design the experiment such that the other two terms do not contribute significantly to the overall uncertainty $\Delta I_o/I_o$. In the next three sections, we will discuss how we deal with these issues.

4.3 Electron Angular Acceptance and Its Contribution to $\Delta I_o/I_o$

We want to keep the contribution to $\Delta I_o/I_o$ from the term $h(\theta_e)\Delta\theta_e$ on the order $\lesssim$ 3%. For fixed kinematical conditions, $h(\theta_e)$ has a fixed value, *i.e.*, the contribution from $h(\theta_e)\Delta\theta_e$ is proportional to the angular acceptance $\Delta\theta_e$; therefore, one can reduce this contribution by reducing $\Delta\theta_e$. In Table V for the kinematics specified in the proposal for CEBAF E89–05, we list the required electron angular acceptances $\Delta\theta_e$ that result in $h(\theta_e)\Delta\theta_e = \pm\ 0.030$. From this table, we see that a choice of $\Delta\theta_e = \pm\ 0.26°$ will ensure $h(\theta_e)\Delta\theta_e \leq 0.030$ for all the proposed Q^2 points. In the next section, we will discuss the effect of this choice of $\Delta\theta_e$ on the counting rates and the statistical uncertainty $\Delta N_e/N_e$.

Table V. $\Delta\theta_e$ for $h(\theta_e)\Delta\theta_e = 0.030$

Q^2 (GeV/c)^2	θ_e (deg)	E (GeV)	$h(\theta_e)$	$\Delta\theta_e$ (deg)
0.30	45.1	0.80	5.865	0.293
0.50	65.7	0.80	4.389	0.392
1.0	45.0	1.6	6.402	0.269
1.5	65.6	1.6	4.755	0.361
2.0	46.6	2.4	6.573	0.262

4.4 Counting Rates and $\Delta N_{double}/N_{double}$

We chose the electron angular acceptances $\Delta\theta_e = \pm\ 0.26°$ and $\Delta\phi_e^v = \pm\ 0.26°$. The angular acceptances of the neutron arm are matched in the way described in Section 4.8 of the proposal for CEBAF E89–05 by taking into account both the kinematic matching and the Fermi spread. We found that a $\Delta\theta_n = \pm\ 2.27° = \pm\ 39.6$ mr will satisfy the horizontal matching for all Q^2 points. The vertical angular acceptance is chosen to be the same as that in the proposal for CEBAF E89–05, *i.e.*, $\Delta\phi_n^v = \pm\ 0.75°$. In Table VI, we give the neutron angular spread in both directions, which shows that our choice of $\Delta\theta_n = \pm\ 2.27°$ and $\Delta\phi_n^v = \pm\ 0.75°$ is justified.

Table VI. Neutron Angular Spread for $\Delta\theta_e = \Delta\phi_e^{\mathrm{v}} = 0.26°$

Q^2 $(\mathrm{GeV})^2$	$^*(\Delta\theta_n)^k$ (deg)	$^*(\Delta\phi_n^{\mathrm{v}})^k$ (deg)	$^\dagger(\Delta\theta_n)^F = (\Delta\phi_n^{\mathrm{v}})^F$ (deg)	$^\ddagger\Delta\theta_n$ (deg)	$^\ddagger\Delta\phi_n^{\mathrm{v}}$ (deg)
0.30	±0.16	±0.12	±2.11	±2.27	±2.23
0.50	±0.12	±0.11	±2.55	±2.67	±2.66
1.0	±0.18	±0.15	±3.29	±3.47	±3.44
1.5	±0.14	±0.11	±4.91	±5.05	±5.02
2.0	±0.18	±0.18	±6.51	±6.69	±6.69

* The superscript k denotes kinematical matching with the electron arm.

† The superscript F denotes Fermi spread.

‡ $\Delta\theta_n = (\Delta\theta_n)^k + (\Delta\theta_n)^n$, and $\Delta\phi_n^{\mathrm{v}} = (\Delta\phi_n^{\mathrm{v}})^k + (\Delta\phi_n^{\mathrm{v}})^F$

The solid angles determined by these angular acceptances are $\Delta\Omega_e = 0.065$ msr and $\Delta\Omega_n = 2.08$ msr. We used MCEEP to estimate the counting rates. In Table VII, we give the triple cross sections $\langle\sigma_3\rangle$ and the doubles-counting rates R_2 for the five Q^2 points. The counting rates are calculated the same way with the same parameters as presented in the proposal for CEBAF E89–05 except that the efficiency of the neutron detector is now that associated with the double coincidence events, which is ~ 0.10 for one of the front analyzing detectors in the neutron polarimeter[21] without shielding. The polarimeter detection efficiency for the triple coincidences in the proposal for CEBAF E89–05 is typically 0.0020 without shielding. In both the triples and the doubles modes, we used the same factor for transmission of neutrons through the Pb–Fe wall.

Given a data acquisition time T, the number of doubles events is

$$N_{double} = T\, R_2 \,, \tag{38}$$

and the contribution from $\Delta N_{double}/N_{double}$ to $\Delta I_o/I_o$ is

$$\frac{\Delta N_{double}}{N_{double}} = \frac{1}{\sqrt{N_{double}}} = \frac{1}{\sqrt{T\,R_2}}, \tag{39}$$

In Fig. 4 for $Q^2 = 1.0$ as an example, we show this term as a function of T for the proposed Q^2 points. Our goal is to keep this term $\Delta N_{double}/N_{double} < 0.02$; in this case, the data aquisition times are given in Table VIII. With the values of $\Delta N_{double}/N_{double}$ in this table, and the uncertainties $h(\theta_e)\Delta\theta_e \sim 3.0\%$, the uncertainty $\Delta I_o/I_o$ is then dominated by $\Delta\epsilon_n/\epsilon_n \lesssim 10\%$, which we discuss in the next section.

Table VII. Triple Cross Section σ_3 and Doubles Counting Rates R_2 with $\Delta p_e/p_e = \pm\, 0.040$

Q^2	θ_e	$\langle\sigma_3\rangle$ (nb/sr^2-MeV)		R_2 (s^{-1})	
(GeV/c)^2	(°)	G*	D*	G*	D*
0.30	45.1	13.9	14.3	0.87	0.90
0.50	65.7	4.56	4.78	0.21	0.21
1.0	45.0	1.80	2.09	0.15	0.17
1.5	65.6	0.35	0.41	0.028	0.032
2.0	46.6	0.22	0.30	0.029	0.039

* G: For Galster parameterization, D: For Dipole parameterization.

Table VIII. Data Acquisition Times and Associated $\Delta N_{double}/N_{double}$ Values

Q^2 $(\mathrm{GeV}/c)^2$	T (hr)	$\Delta N_{double}/N_{double}$ (%) Gaster	Dipole
0.30	4	0.89	0.88
0.50	12	1.0	1.0
1.0	16	1.1	1.0
1.5	38	1.6	1.5
2.0	36	1.6	1.4

4.5 Neutron Detection Efficiency and Its Uncertainties

The neutron detection efficiency can be calculated from the Monte Carlo code of Cecil, Anderson, and Madey[21] with a relative uncertainty of about ±5%; however, we want to measure this detection efficiency not only as a check on the calculation, but more importantly to endeavor to reduce the relative uncertainty. The neutron detection efficiency can be determined by means of the associated-particle technique. For this experiment, we plan to measure the efficiency *via* the following reaction:

$$\gamma + p \rightarrow \pi^+ + n \,. \tag{40}$$

We plan to use electron beam to provide virtual photons with sufficient energy E_γ to generate neutrons that will have the same momenta as those in the proposal for CEBAF E89–05 at the neutron angles given in that proposal. For known neutron momentum p_n and scattering angle θ_n, energy and momentum conservation laws lead to

$$E_\gamma = \frac{2M_p\sqrt{p_n^2 + M_n^2} + M_\pi^2 - M_p^2 - M_n^2}{2\,(M_p - \sqrt{p_n^2 + M_n^2} + p_n \cos\theta_n)}, \tag{41}$$

$$p_\pi = p_n\sqrt{1 - 2(E_\gamma/p_n)\cos\theta_n + (E_\gamma/p_n)^2}, \tag{42}$$

and

$$\sin\theta_\pi = \frac{\sin\theta_n}{\sqrt{1 - 2(E_\gamma/p_n)\cos\theta_n + (E_\gamma/p_n)^2}}. \tag{43}$$

In Table IX, we show E_γ, p_π, and θ_π corresponding to the neutron momenta and scattering angles designed for this experiment. In this reaction, the positive pions will be counted in the HMS (with polarity reversed from that for electrons), and the neutrons will be counted in coincidence with the pions. The neutron detection efficiency is simply the ratio of the measured pion-neutron coincidence rate to the measured inclusive single-arm pion rate.

Table IX. E_γ, p_π, and θ_π in reaction $\gamma p \to \pi^+ n$

p_n (MeV/c)	T_n (MeV)	θ_n (deg)	E_γ (MeV)	p_π (MeV/c)	T_π (MeV)	θ_π (deg)
572	160	52.3	852	676	551	42.0
757	267	39.8	831	545	423	62.8
1133	532	41.2	1597	1054	924	45.1
1464	799	29.8	1621	808	680	64.3
1771	1063	33.1	2420	1346	1213	45.9

The validity of this associated–particle technique depends on the ability to discriminate against processes that contaminate the single–arm rate; for example, photons with energies listed in Table IX will trigger the two–pion process $\gamma p \to \pi^+\pi^\circ n$ because the threshold energy for this process is $E_{th} \simeq 316$ MeV; however, negative pions from the two–pion process with appropriate momentum and angle require a beam energy of about 140 MeV higher than the E_γ values listed in Table IX. By choosing a beam energy to be ~970 MeV for $Q^2 = 0.30$ and 0.50 (GeV/c)^2, ~1740 MeV for $Q^2 = 1.0$ and 1.5 (GeV/c)^2, and ~2550 MeV for $Q^2 = 2.0$ (GeV/c)^2, we avoid contamination from positive pions produced in the two–pion production process. We used CELEG to study the single- and double–pion processes. Because the dominant contribution to the relative uncertainty

in I_o is the uncertainty in ϵ_n, we expect an efficiency measurement with relative uncertainties of $\sim 5\%$, which translates to a relative uncertainty in G_M^n of $\sim 3\%$, as shown later in Table XIV.

4.6 Measurement of the Neutron Detection Efficiency

To measure the efficiency *via* the $\gamma\, p \rightarrow \pi^+\, n$ reaction, the pion count rates can be estimated from

$$R_\pi = L \left(\frac{d\sigma_e}{d\Omega_\pi} \right) \Delta\Omega_\pi, \tag{44}$$

where the luminosity

$$L(\mathrm{cm}^{-2}\mathrm{s}^{-1}) = F \left(\frac{N_o\, \rho\, x}{A} \right) \tag{45}$$

and

F = incident flux of electrons that emit photons to trigger the reaction $\gamma\, p \rightarrow \pi\, n$, (electron/s)

N_o = Avogadro's number (6.022×10^{23} nuclei/mole)

ρx = target thickness of LH_2 [(= 0.070 g/cc)(5 cm) = 0.35 g/cm^2 LH_2]

$d\sigma_e/d\Omega_\pi$ = pion production cross section induced by an electron of energy E with a pion being scattered at an angle θ_π into a solid angle $\Delta\Omega_\pi$. It has units of cm^2/sr. This cross section can be related to the photon induced cross section $d\sigma_\gamma/d\Omega_\pi$ in terms of an equivalent virtual photon spectrum. We will dicuss it below.

$\Delta\Omega_\pi$ = the pion solid angle, sr. In efficiency measurements, we plan to collimate the HMS (which now detects positive pions) in the same way as that in the I_o measurements (*i.e.* $\Delta\Omega_n = \Delta\Omega_e = 0.0647$ msr).

In dealing with pion electroproduction, the concept of a virtual photon spectrum, originated by Weizsäcker[23] and Williams[24], has been used extensively to relate nuclear excitaions induced by electron scattering to the same excitations

induced by photons. In such experiments the final electron is not detected and the target is bathed in a spectrum of virtual photons. In this picture, the electroproduction of pions to certain final states is decribed equivalently by photoproduction of pions to the same final states:[25]

$$\frac{d\sigma_e(E)}{d\Omega_\pi} = \int_{E_\gamma^-}^{E_\gamma^+} \frac{dN_\gamma(E,E_\gamma)}{dE_\gamma})\frac{d\sigma_\gamma(E_\gamma)}{d\Omega_\pi})\, dE_\gamma, \tag{46}$$

where $dN_\gamma(E,E_\gamma)/dE_\gamma$ is the virtual photon flux (per unit of photon energy). For our purpose of count rate estimation, this expression is approximated

$$\frac{d\sigma_e(E)}{d\Omega_\pi} = \frac{d\sigma_\gamma(E_\gamma^c)}{d\Omega_\pi} \int_{E_\gamma^-}^{E_\gamma^+} \frac{dN_\gamma(E,E_\gamma)}{dE_\gamma}\, dE_\gamma = N_\gamma \frac{d\sigma_\gamma(E_\gamma^c)}{d\Omega_\pi} \tag{47}$$

where E_γ^c is the center value of the energy band between $E_\gamma^- < E_\gamma < E_\gamma^+$, and

$$N_\gamma = \int_{E_\gamma^-}^{E_\gamma^+} \frac{dN_\gamma(E,E_\gamma)}{dE_\gamma}\, dE_\gamma, \tag{48}$$

which is the number of equivalent photons within the photon energy band. In this expression, the photon flux can be written as[25]

$$\frac{dN_\gamma(E,E_\gamma)}{dE_\gamma} = \frac{f_\gamma(E_\gamma)}{E_\gamma}, \tag{49}$$

where the function $f_\gamma(E_\gamma)$ is known as virtual photon spectrum and has been modeled by Tiator and Wright.[25] . In view of Eqs. (44) and (47), the pion count rate can be estimated by

$$R_\pi = L\, N_\gamma \left(\frac{d\sigma_\gamma}{d\Omega_\pi}\right) \Delta\Omega_\pi, \tag{50}$$

To compute N_γ, we used Tiator-Wright model in which $f_\gamma(E_\gamma)$ can be evaluated in the forward-peaking approximation for the given kinematics in an experiment.

The expression for $f_\gamma(E_\gamma)$ depends on E_γ:

$$f_\gamma = C_1 E_\gamma^2 - C_2, \tag{51}$$

where the constants C_1 and C_2 are related to the variables given in the appendix of Ref. 26 by rather complicated formulas [which we do not show here]. Now the equivalent virtual photon number can be calculated

$$N_\gamma = \int_{E_\gamma^-}^{E_\gamma^+} \left(\frac{f_\gamma}{E_\gamma}\right) dE_\gamma = \frac{C_1}{2}\left[(E_\gamma^+)^2 - (E_\gamma^-)^2\right] - C_2 \ln \frac{E_\gamma^+}{E_\gamma^-}, \tag{52}$$

where the upper limit of photon energy E_γ^+ is determined by the smaller of the electron beam energy or the value calculated from Eq. (41) with $\theta_n \to \theta_n + \Delta\theta_n$, while the lower limit E_γ^- is determined by Eq. (41) with $\theta_n \to \theta_n - \Delta\theta_n$.

The pion photoproduction cross sections have been measured by various groups[26,27,28] for the reaction $\gamma p \to \pi^+ n$ in our energy region. Although the published data were not at exactly the same kinematic conditions as ours, the values of cross section for our kinematics can be extrapolated within less than one order of magnitude from the published data. In Table X, we list these roughly extrapolated values for the cross section.

Table X. Estimated pion photoproduction cross section values

E_γ (MeV)	$(\theta_\pi)_{lab}$ (deg)	$(\theta_\pi)_{c.m.}$ (deg)	$\frac{d\Omega_{c.m.}}{d\Omega_{lab}}$	$\left(\frac{d\sigma_\gamma}{d\Omega_\pi}\right)_{c.m.}$ (μb/sr)	$\left(\frac{d\sigma_\gamma}{d\Omega_\pi}\right)_{lab}$ (μb/sr)
852	42.0	66.4	0.53	$\sim 5^*$	~ 3
831	62.8	92.0	0.79	$\sim 5^*$	~ 4
1597	45.1	82.7	0.51	$\sim 1^\dagger$	~ 0.5
1621	64.3	106.7	0.89	$\sim 0.5^\ddagger$	~ 0.4
2420	45.9	93.1	0.51	$\sim 0.05^\ddagger$	~ 0.03

* Extrapolated from Ref. 27 rather accurately.

† Estimated from Ref. 28.

‡ Roughly estimated from Ref. 29.

Now, we give in Table XI the quantities needed by Eq. (50) and the values of the estimated count rates.

Table XI. Values of the quantities used in Eq. (50) and count rates with $L = 2.6 \times 10^{38}$ cm^{2}s^{-1} and $\Delta\Omega_\pi = 0.0647$ msr

p_π (MeV/c)	θ_π (deg)	E_γ^c (MeV)	E_γ^+ (MeV)	E_γ^- (MeV)	N_γ ($\times 10^{-4}$)	$\frac{d\sigma_\gamma}{d\Omega_\pi}$ (nb/sr)	R_π (s^{-1})
676	42.0	852	970	759	9.72	~ 3	~ 49
545	62.8	831	907	770	7.98	~ 4	~ 54
1054	45.1	1597	1740	1423	9.17	~ 0.5	~ 7.8
808	64.3	1621	1740	1504	6.83	~ 0.4	~ 4.7
1346	45.9	2420	2550	2167	34.1	~ 0.03	~ 1.7

The detection efficiency of the neutron arm (including the neutron polarimeter

and the front shielding wall) is

$$\epsilon_n = \epsilon\, t = \frac{R_{n\pi}}{R_\pi}, \tag{53}$$

where ϵ is the neutron detection efficiency of a "bare" neutron detector, $t \sim 0.40$ is the transmission coefficient of neutrons through the shielding wall, $R_{n\pi} = R_\pi \epsilon_n$ is the neutron-pion coincidence rate with the whole neutron detecting system. Obviously, $R_{n\pi} = R_\pi$ for an ideal neutron detecting system with detection efficiency ϵ_n of unity. The relative statistical uncertainty is

$$\left(\frac{\Delta\epsilon_n}{\epsilon_n}\right)_{stat} = \left[\left(\frac{\Delta R_{n\pi}}{R_{n\pi}}\right)^2 + \left(\frac{\Delta R_\pi}{R_\pi}\right)^2\right]^{1/2} \tag{54}$$

For a given data aquisition time T, $R_{n\pi} = N_{n\pi}/T$ and $R_\pi = N_\pi/T$ where $N_{n\pi}$ and N_π are the total number of neutron-pion coincidence events and single-arm pions detected, respectively. Thus, $\Delta R_{n\pi}/R_{n\pi} = \Delta N_{n\pi}/N_{n\pi}$ and $\Delta R_\pi/R_\pi = \Delta N_\pi/N_\pi$, and

$$\left(\frac{\Delta\epsilon_n}{\epsilon_n}\right)_{stat} = \left[\left(\frac{\Delta N_{n\pi}}{N_{n\pi}}\right)^2 + \left(\frac{\Delta N_\pi}{N_\pi}\right)^2\right]^{1/2} = \left(\frac{1}{N_{n\pi}} + \frac{1}{N_\pi}\right)^{1/2}. \tag{55}$$

For a single detector in the neutron polarimeter without shielding, the neutron detection efficiency is estimated to be $\epsilon \sim 10\%$; therefore, with the shielding wall $N_{n\pi} \simeq \epsilon\, t\, N_\pi$. Then for a given data aquisition time T, we have

$$\left(\frac{\Delta\epsilon_n}{\epsilon_n}\right)_{stat} \simeq \left(\frac{1}{\epsilon\, t\, N_\pi} + \frac{1}{N_\pi}\right)^{1/2} = y \times \frac{1}{60 \times \sqrt{T\,(\mathrm{hr})}}, \tag{56}$$

where

$$y(\mathrm{sec})^{1/2} = \sqrt{\frac{1}{R_\pi}\left(1 + \frac{1}{\epsilon\, t}\right)} \simeq \sqrt{\frac{26}{R_\pi}} \simeq \frac{5.1}{\sqrt{R_\pi}} \tag{57}$$

We want $(\Delta\epsilon_n/\epsilon_n)_{stat} \sim 0.01$. In Table XII, we give the values of y, the data acquisition time T, and the relative statistical uncertainty $(\Delta\epsilon_n/\epsilon_n)_{stat}$

Table XII. The value of y, the data acquistion time T, and the relative statistical uncertainty in ϵ_n

Q^2 $(\mathrm{GeV/c})^2$	y $(\mathrm{sec})^{1/2}$	T (hr)	$(\Delta\epsilon_n/\epsilon_n)_{stat}$ (%)
0.30	0.723	2	0.85
0.50	0.692	2	0.82
1.0	1.83	10	0.96
1.5	2.36	16	0.99
2.0	6.69	25	1.28

Although Table XII shows that a relatively short time is needed to obtain small statistical uncertainties for the four lower Q^2 points, we plan to request data acquisition times about three times those in the this table because the rough extrapolation of the cross section may be one order of magnitude off, which will contribute to the uncertainty by either a factor of ~ 3 or $\sim 1/3$ [Note that the uncertainty is inversely proportional to the square root of the cross section].

4.7 Projected Uncertainties in I_o and G_M^n

With a conservative value of $\Delta\epsilon_n/\epsilon_n = 0.10$ and a less conservative value of $\Delta\epsilon_n/\epsilon_n = 0.05$, we calculated various contributing terms in the uncertainties $\Delta I_o/I_o$ and $\Delta G_M^n/G_M^n$. In the calculation, we use $\Delta\theta_e = \pm\ 0.26°$ and the projected values of $\Delta D_{LS'}/D_{LS'}$ given in the proposal for CEBAF E89-05. In the actual experiment, the values of $D_{LS'}$ will assume the values obtained from the $P_{S'}$ measurements as proposed for CEBAF E89-05. In Tables XIII(a) and XIII(b), we present the uncertainty contributions to $\Delta I_o/I_o$; and in Tables XIV(a) and XIV(b) we give the final projected uncertainties in G_M^n, which are also shown in Fig. 5. It should be noted that the projected uncertainties in G_M^n are dominated by the uncertainties in I_o, which in turn are dominated by the uncertainties in the neutron detection efficiency. [In the worst case, we expect $\sim 10\%$ uncertainty in ϵ_n;

therefore, the actual experimental uncertainties in G_M^n will most likely be smaller than those given in Table XIV(a), and we expect that they will be close to or better than those in Table XIV(b)]

Table XIII(a). Projected Uncertainties in I_o with $\Delta\theta_e = \pm\, 0.26°$ and $\Delta\epsilon_n/\epsilon_n = 0.10$

Q^2	θ	E	$\Delta N_{double}/N_{double}$ (%)		$h(\theta_e)\Delta\theta_e$ (%)	$\Delta I_o/I_o$ (%)	
$(\mathrm{GeV}/c)^2$	(deg)	(GeV)	G*	D*		G*	D*
2.0	46.6	2.4	1.59	1.56	2.66	10.5	10.5
1.5	65.5	1.6	1.89	1.84	1.99	10.4	10.4
1.0	45.0	1.6	1.92	1.79	2.91	10.6	10.6
0.5	65.5	0.8	2.05	1.90	2.16	10.4	10.4
0.3	45.0	0.8	2.03	1.76	2.98	10.6	10.6

Table XIII(b). Projected Uncertainties in I_o with $\Delta\theta_e = \pm\, 0.26°$ and $\Delta\epsilon_n/\epsilon_n = 0.05$

Q^2	θ	E	$\Delta N_{double}/N_{double}$ (%)		$h(\theta_e)\Delta\theta_e$ (%)	$\Delta I_o/I_o$ (%)	
$(\mathrm{GeV}/c)^2$	(deg)	(GeV)	G*	D*		G*	D*
2.0	46.6	2.4	1.59	1.56	2.66	5.9	5.9
1.5	65.5	1.6	1.89	1.84	1.99	5.8	5.8
1.0	45.0	1.6	1.92	1.79	2.91	6.1	6.1
0.5	65.5	0.8	2.05	1.90	2.16	5.8	5.8
0.3	45.0	0.8	2.03	1.76	2.98	6.1	6.1

Table XIV(a). Projected Uncertainties in G_M^n with $\Delta\theta_e = \pm\, 0.26°$ and $\Delta\epsilon_n/\epsilon_n = 0.10$

Q^2 (GeV/c)^2	θ (deg)	E (GeV)	$\Delta I_o/I_o$ (%)	$\Delta G_M^n/G_M^n$ (%) G^*	D^*
2.0	46.6	2.4	10.5	5.0	5.0
1.5	65.5	1.6	10.4	5.2	5.2
1.0	45.0	1.6	10.6	5.3	5.6
0.50	65.5	0.80	10.4	5.3	5.7
0.30	45.0	0.80	10.6	5.4	5.7

Table XIV(b). Projected Uncertainties in G_M^n with $\Delta\theta_e = \pm\, 0.26°$ and $\Delta\epsilon_n/\epsilon_n = 0.050$

Q^2 (GeV/c)^2	θ (deg)	E (GeV)	$\Delta I_o/I_o$ (%)	$\Delta G_M^n/G_M^n$ (%) G^*	D^*
2.0	46.6	2.4	5.9	3.0	3.1
1.5	65.5	1.6	5.8	3.2	3.0
1.0	45.0	1.6	6.1	3.1	3.8
0.50	65.5	0.80	5.8	3.0	3.8
0.30	45.0	0.80	6.1	3.2	3.9

* G (D): with the Galster (Dipole) parameterization of G_E^n.

5. Background Processes

(see Section 5 of the proposal for CEBAF E89-05)

6. Beam Time Request

We propose to measure G_M^n at $Q^2 = 1.0$ (GeV/c)^2 initially in conjunction eith our proposed intial measurement of G_E^n and then to make measurements at each of the other Q^2 points when we schedule the G_E^n runs. The additional beam time requested for a measurement of G_M^n at $Q^2 = 1.0$ (GeV/c)^2 with a luminosity of 3.2×10^{38} cm^{-2}s^{-1} is as follows:

Activity		Beam on Target(hr)
1. Checkout with small collimator		**16**
1.1 Electron spectrometer		
1.2 Neutron polarimeter		
1.3 Electron–neutron coincidences		
2. Data acquisition: Measurement of I_o		**20**
2.1 LD_2 target	8	
2.2 Dummy target cell	4	
2.3 Shadow shield(with LD_2 target)	4	
2.4 LH_2 target	4	
3. Data acquisition: Efficiency measurement with a LH_2 target		**30**
4. Overhead and Contingency		**14**
TOTAL		**80**

The total additional beam time required to measure G_M^n at all five Q^2 points is as follows (see next page)

Q^2 (GeV/c)^2	Time to measure I_0 (hrs)	Time to measure ϵ_n (hrs)	Checkout time (hrs)	Overhead & contingency (hrs)	Total time (hrs)
0.30	20	8	16	12	56
0.50	20	8	16	12	56
Subtotal A	*40*	*16*	*32*	*24*	*108*
1.0	20	30	16	14	80
1.5	60	48	16	24	148
2.0	60	75	16	30	181
Subtotal B	*140*	153	*48*	*68*	*409*
TOTAL	180	169	80	72	521

References

1. H. Arenhövel, Phys. Lett. **B199**, 13 (1987).
2. M. P. Rekalo, G. I. Gakh, and A. P. Rekalo, J. Phys. G: Nucl. Part. Phys. **15**, 1223 (1989).
3. B. Mosconi and P. Ricci, Nucl. Phys. **A517**, 483 (1990); G. Beck and H. Arenhövel, Few-Body Systems **13**, 165 (1992).
4. J. M. Laget, Phys. Lett. **B273**, 367 (1991).
5. A. Lung *et al.*, Phys. Rev. Lett. **70**, 718 (1993).
6. A. S. Esaulov *et al.*, Sov. J. Nucl. Phys. **45**, 258 (1987).
7. W. Bartel *et al.*, Nucl. Phys. **B58**, 429 (1973).
8. K. M. Hanson *et al.*, Phys. Rev. **D8**, 753 (1973).
9. W. Albrecht *et al.*, Phys. Lett. **26B**, 642 (1968).
10. J. R. Dunning *et al.*, Phys. Rev. **141**, 1286 (1966).
11. P. Stein *et al.*, Phys. Rev. Lett. **16**, 592 (1966).
12. E. B. Hughes *et al.*, Phys. Rev. **139**, B458 (1965).
13. C. W. Akerlof *et al.*, Phys. Rev. **135**, B810 (1964).
14. S. Rock *et al.*, Phys. Rev. Lett. **49**, 1139 (1982).
15. R. V. Reid, Ann. Phys. (N.Y.) **50**, 411 (1968).
16. M. Lacombe *et al.*, Phys. Lett. **101B**, 139 (1981); Phys. Rev. C**21**, 861 (1980).
17. W. W. Buck and F. Gross, Phys. Rev. D**20**, 2361 (1979).
18. P. Markowitz *et al.*, to be published.
19. I. Sick, Nucl. Phys. **A497**, 379c (1989).
20. R. G. Arnold, C. E. Carlson, F. Gross, Phys. Rev. **23**, 363 (1981).

21. R. Cecil, B. D. Anderson, R. Madey, Nucl. Instr. and Meth. **161**, 439 (1979).

22. J. W. Lightbody, Jr. and J. S. Connell, R. Madey, Computers in Physics, May/June, 57 (1988).

23. C. F. Weizsäker, Z. Phys. **88**, 612 (1934).

24. E. J. Williams, Mat. Pys. Medd. Dan. Vid. Selsk. **13**, No. 4(1935).

25. L. E. Wright and L. Tiator, Phys. Rev. C**26**, 2349(1982); L. Tiator and L. E. Wright, Nucl. Phys. C**374**, 401(1982).

26. S. D. Ecklund and R. L. Walker, Phys. Rev. **159**, 1195(1967).

27. G. Buschhorn *et al.,* Phys Rev. Lett. **17**, 1027(1966).

28. G. Buschhorn *et al.,* Phys Rev. Lett. **18**, 571(1966).

Appendix

World's Data Set for G_M^n (for $0.30 \leq Q^2$ (GeV/c)$^2 \leq 2.0$)

We present the world's data set for the magnetic form factor of the neutron, as compiled from the literature in the Q^2 range of 0.3–2.0 (GeV/c)^2. The succeeding table will present G_M^n/μ_n ($\mu_n = -1.91$) and its uncertainty in ascending order with respect to Q^2. A superscript number by the value of G_M^n/μ_n denotes the reference in the bibliography.

World's Data set for G_M^n

Q^2 (GeV/c)^2	G_M^n/μ_n	$\Delta(G_M^n/\mu_n)$	$\Delta(G_M^n/\mu_n)/(G_M^n/\mu_n)$
0.389	0.405[7]	0.038	0.094
0.389	0.445[10]	0.021	0.047
0.390	0.413[8]	0.011	0.027
0.390	0.432[11]	0.034	0.079
0.390	0.432[12]	0.042	0.097
0.429	0.387[13]	0.063	0.163
0.482	0.348[6]	0.045	0.129
0.488	0.382[12]	0.042	0.110
0.545	0.320[6]	0.043	0.134
0.565	0.313[7]	0.025	0.080
0.566	0.334[11]	0.022	0.066
0.585	0.283[8]	0.017	0.060
0.585	0.331[12]	0.038	0.115
0.585	0.309[13]	0.052	0.168
0.608	0.362[6]	0.042	0.116

World's Data set for G_M^n (cont'd)

Q^2 (GeV/c)^2	G_M^n/μ_n	$\Delta(G_M^n/\mu_n)$	$\Delta(G_M^n/\mu_n)/(G_M^n/\mu_n)$
0.623	0.310[10]	0.021	0.068
0.646	0.307[6]	0.042	0.137
0.692	0.278[6]	0.042	0.151
0.702	0.265[9]	0.020	0.754
0.780	0.227[7]	0.012	0.053
0.780	0.179[8]	0.013	0.073
0.780	0.249[12]	0.049	0.198
0.780	0.204[13]	0.047	0.230
0.832	0.220[6]	0.042	0.191
0.857	0.218[10]	0.028	0.128
0.975	0.224[12]	0.040	0.176
0.975	0.126[13]	0.045	0.357
1.000	0.168[7]	0.009	0.054
1.010	0.188[9]	0.012	0.064
1.170	0.136[8]	0.006	0.044
1.170	0.183[10]	0.021	0.115
1.170	0.156[12]	0.041	0.263
1.530	0.106[7]	0.006	0.057
1.750	0.087[5]	0.005	0.057
1.750	0.120[10]	0.011	0.092
1.755	0.083[8]	0.006	0.072
1.845	0.083[9]	0.006	0.072

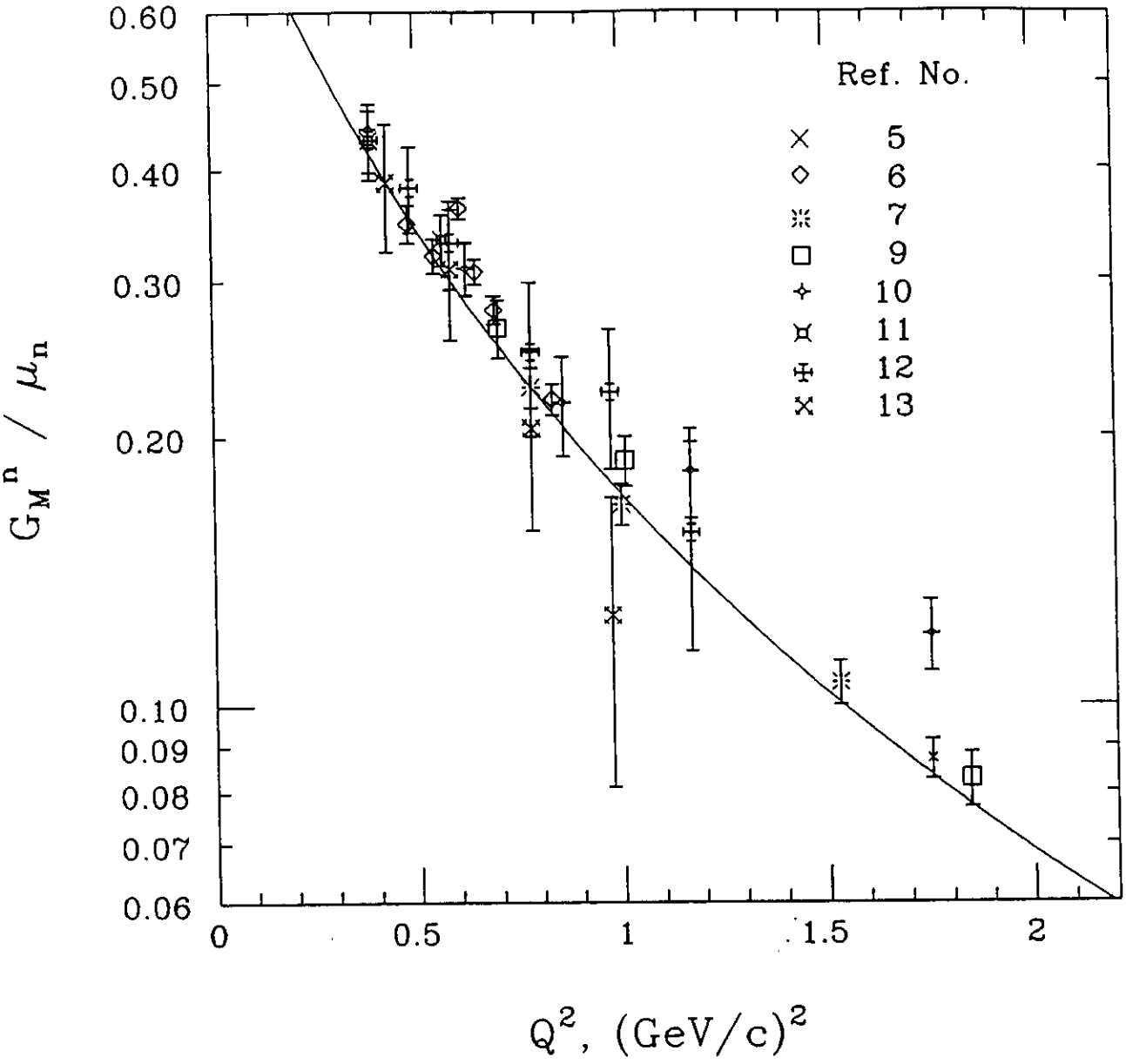

Fig. 1 Results of G_M^n from Previous Measurements.

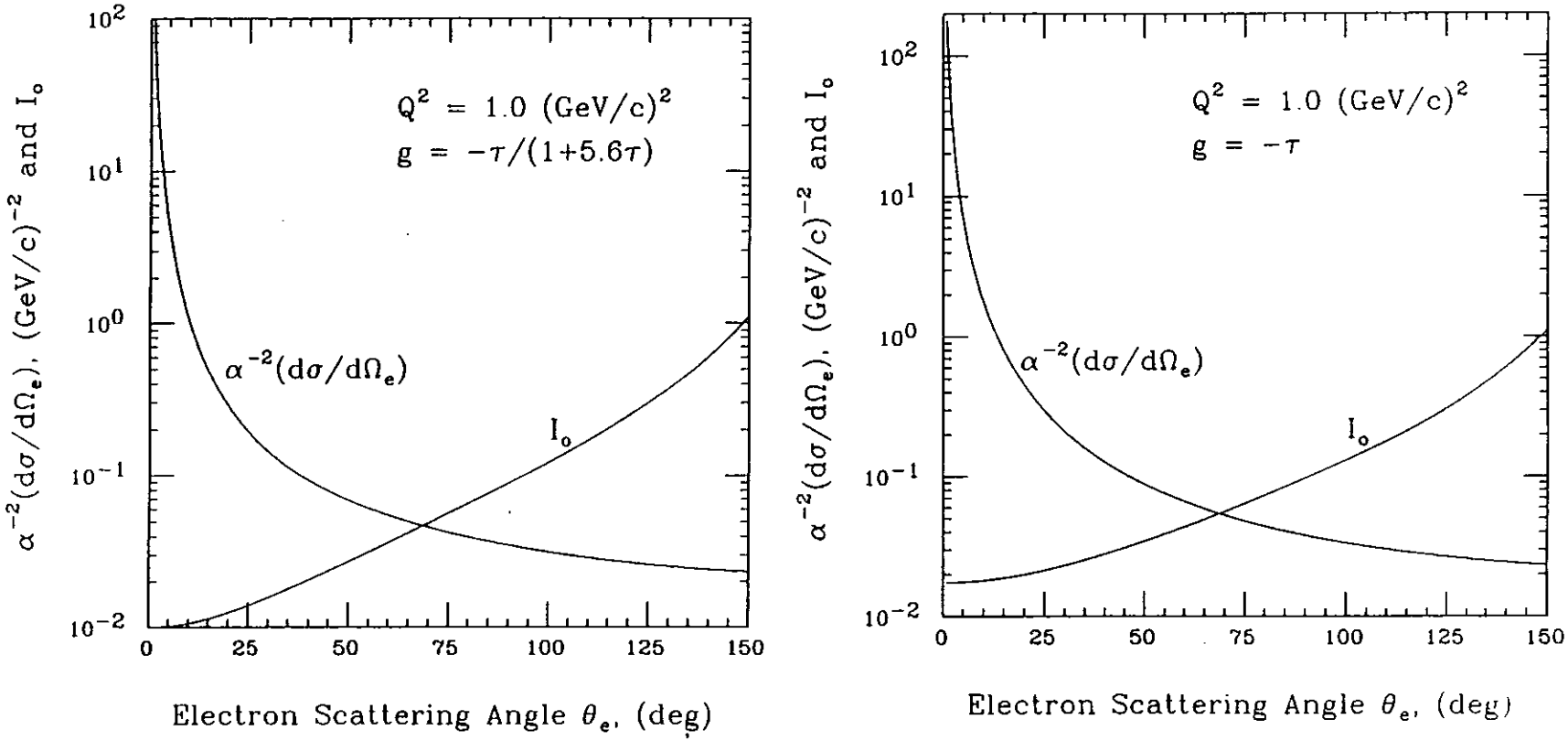

Fig. 2 $d\sigma/d\Omega_e$ and I_o vs Electron Angle θ_e for $Q^2 = 1.0$ (GeV/c)^2.

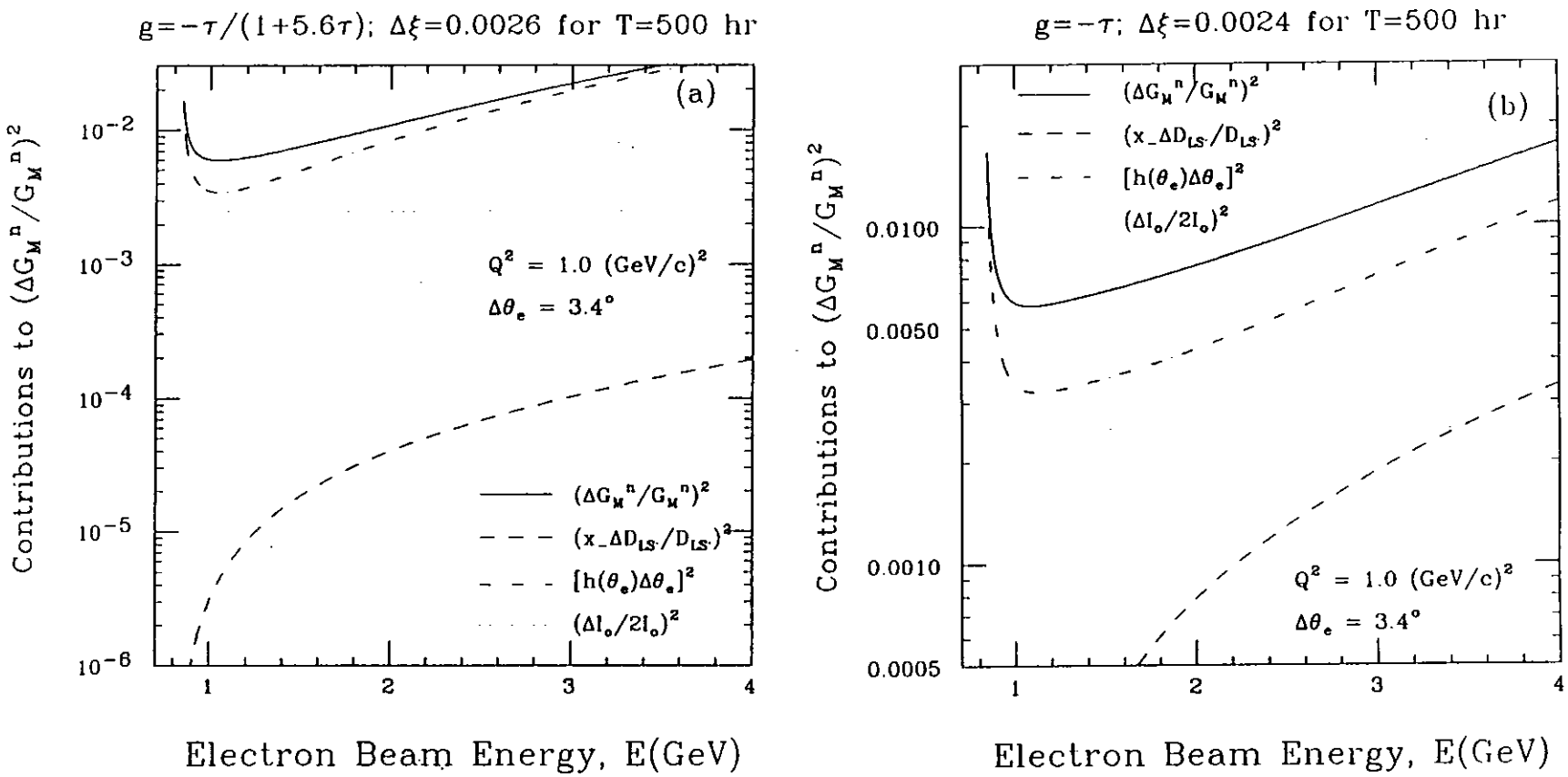

Fig. 3 Contributions to $(\Delta G_M^n/G_M^n)^2$ for $Q^2 = 1.0$ (GeV/c)^2.

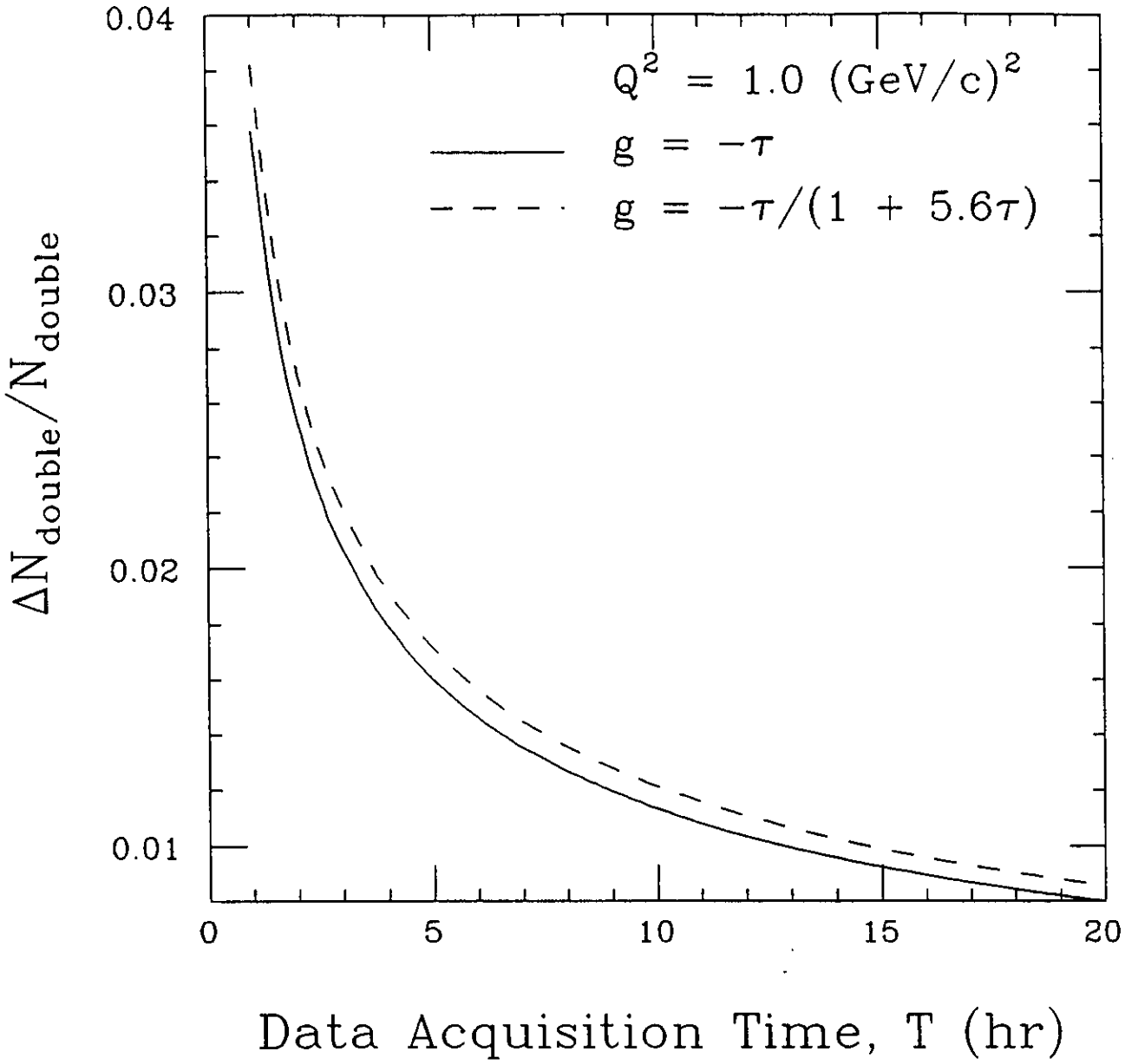

Fig. 4 $\Delta N_{double}/N_{double}$ vs T for $Q^2 = 1.0$ (GeV/c)^2.

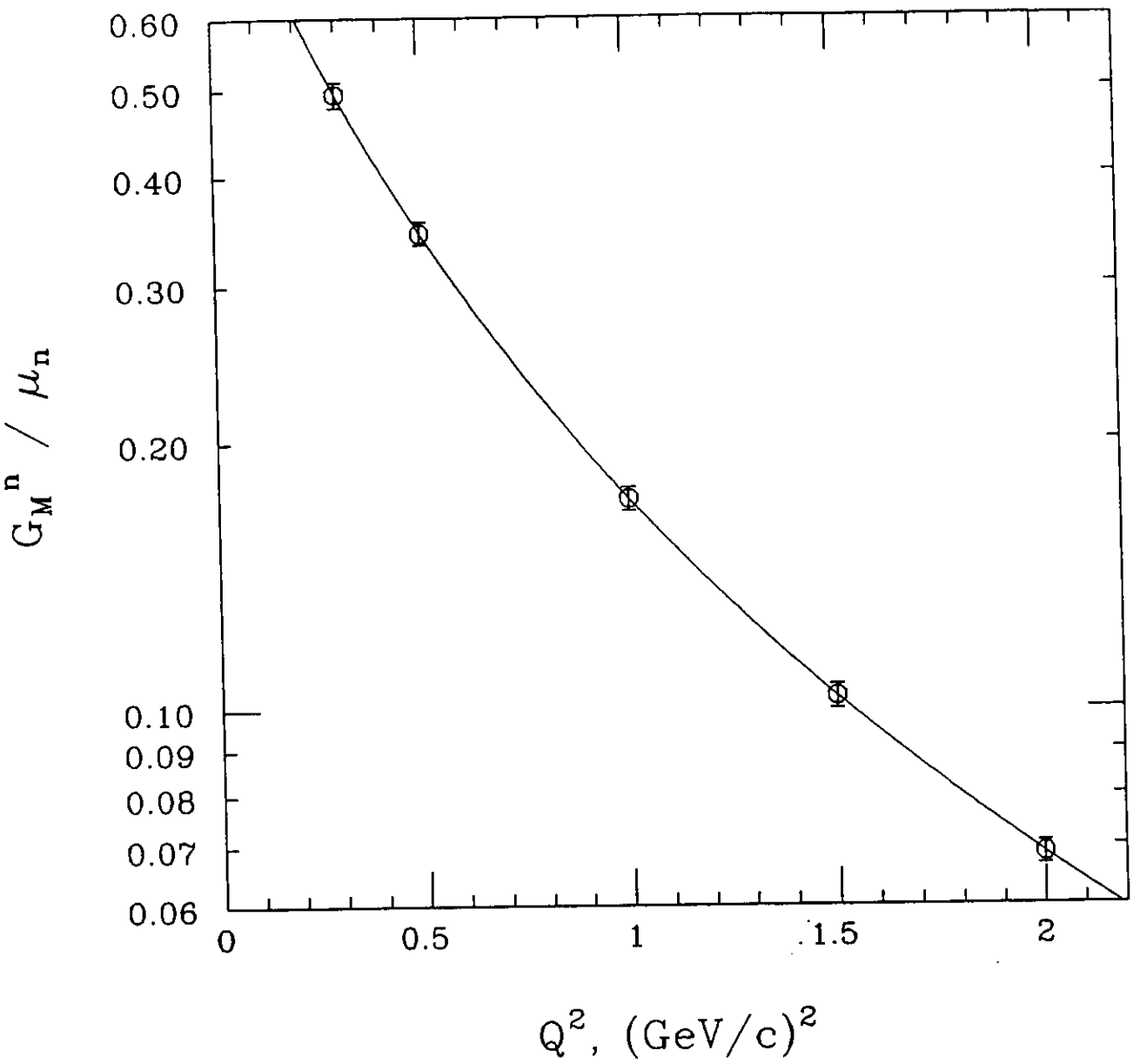

Fig. 5 G_M^n with Projected Uncertainty ΔG_M^n vs Q^2.